Brain Stimulation 18 (2025) 265–275

Contents lists available at ScienceDirect

Brain Stimulation

journal homepage: www.journals.elsevier.com/brain-stimulation

Pulsed inhibition of corticospinal excitability by the thalamocortical sleep spindle

Umair Hassan [a,b,c,d,*], Prince Okyere [a,e], Milad Amini Masouleh [a,f,g], Christoph Zrenner [h,i], Ulf Ziemann [j,k], Til Ole Bergmann [a,b,**]

[a] Neuroimaging Center (NIC), Focus Program Translational Neuroscience (FTN), Johannes Gutenberg University Medical Center, Mainz, Germany
[b] Leibniz Institute for Resilience Research (LIR), Mainz, Germany
[c] Department of Psychiatry and Behavioral Sciences, Stanford School of Medicine, Stanford University, USA
[d] Wu-Tsai Neurosciences Institute, Stanford University, USA
[e] School of Psychology, University of Surrey, Guildford, UK
[f] Department of Psychology and Neurosciences, Leibniz Research Centre for Working Environment and Human Factors (IfADo), Ardeystraße 67, Dortmund, Germany
[g] Psychology Department, Ruhr University Bochum, Bochum, Germany
[h] Temerty Centre for Therapeutic Brain Intervention, Centre for Addiction and Mental Health, Toronto, Canada
[i] Department of Psychiatry, Faculty of Medicine, And Institute for Biomedical Engineering, And Institute of Medical Science, University of Toronto, Toronto, Canada
[j] Department of Neurology & Stroke, Eberhard Karls University of Tübingen, Tübingen, Germany
[k] Hertie Institute for Clinical Brain Research, Eberhard Karls University of Tübingen, Tübingen, Germany

A B S T R A C T

Thalamocortical sleep spindles, i.e., oscillatory bursts at ~12–15 Hz of waxing and waning amplitude, are a hallmark feature of non-rapid eye movement (NREM) sleep and believed to play a key role in memory reactivation and consolidation. Generated in the thalamus and projecting to neocortex and hippocampus, they are phasically modulated by neocortical slow oscillations (<1 Hz) and in turn phasically modulate hippocampal sharp-wave ripples (>80 Hz). This hierarchical cross-frequency nesting, where slower oscillations group faster ones into certain excitability phases, may enable phase-dependent plasticity in the neocortex, and spindles have thus been considered windows of plasticity in the sleeping brain. However, the assumed phasic excitability modulation had not yet been demonstrated for spindles. Utilizing a recently developed real-time spindle detection algorithm, we applied spindle phase-triggered transcranial magnetic stimulation (TMS) to the primary motor cortex (M1) hand area to characterize the corticospinal excitability profile of spindles via motor evoked potentials (MEP). MEPs showed net suppression during spindles, driven by a "pulse of inhibition" during its falling flank with no inhibition or facilitation during its peak, rising flank, or trough. This unidirectional ("asymmetric") modulation occurred on top of the general sleep-related inhibition during spindle-free NREM sleep and did not extend into the refractory post-spindle periods. We conclude that spindles exert "asymmetric pulsed inhibition" on corticospinal excitability. These findings and the developed real-time spindle targeting methods enable future studies to investigate the causal role of spindles in phase-dependent synaptic plasticity and systems memory consolidation during sleep by repetitively targeting relevant spindle phases.

1. Introduction

Thalamocortical sleep spindles are transient oscillatory complexes of waxing and waning amplitude at sigma frequency (~12–15 Hz) and constitute a hallmark feature of the electroencephalogram (EEG) during non-rapid eye movement (NREM) sleep. Nested phase–amplitude coupling of spindles with 0.5–1 Hz neocortical slow oscillations (SOs) and hippocampal ripples (>80 Hz) (Staresina et al., 2015) facilitates sleep-dependent memory reactivation [1] and systems consolidation [2], thus endorsing the concepts of phase-dependent plasticity [3] and synaptic rescaling of cortical neurons [4]. Sleep spindles are generated by the reciprocal interaction of inhibitory reticular-thalamic and excitatory corticothalamic neurons [5], while their initiation and termination may involve both excitatory corticothalamic [6–11] and inhibitory reticular-thalamic neurons [12–14]. These mechanisms of spindle generation and termination likely cause rhythmic fluctuations in the excitation/inhibition balance (EIB) of neocortical neuron populations [15–17] that have also been linked to processes of synaptic rescaling and systems memory consolidation [4,18].

While phasic corticospinal excitability fluctuations have already been demonstrated in humans using real-time EEG triggered transcranial magnetic stimulation (TMS) of the primary motor cortex (M1)

* Corresponding author;Leibniz Institute for Resilience Research (LIR), Mainz, Germany
** Corresponding author;Leibniz Institute for Resilience Research (LIR), Mainz, Germany
E-mail addresses: umair.hassan@stanford.edu, umairhassankhanniazi@gmail.com (U. Hassan), tobergmann@uni-mainz.com (T.O. Bergmann).

https://doi.org/10.1016/j.brs.2025.02.015
Received 27 July 2024; Received in revised form 30 January 2025; Accepted 18 February 2025
Available online 21 February 2025

and assessment of motor evoked potential (MEP) modulations for the sensorimotor mu-alpha oscillation during wakefulness [19,20] as well as the SO during deep sleep [21], a similar phasic modulation remained yet to be shown for sleep spindles. Here, we conducted a first investigation into the corticospinal excitability dynamics during spontaneously occurring sleep spindles in humans using a recently developed real-time spindle detection algorithm [22] to trigger TMS of the left M1 hand area and assess MEP amplitudes. We probed excitability close to the spindle center during four different phase angles (trough, rising flank, peak, falling flank) as well as during the refractory period immediately following spindles and during baseline periods of desynchronized low amplitude NREM sleep where spindles and SO were absent (Fig. 1B).

This set of conditions and the inclusion of a spindle-free (i.e., low-sigma power) baseline allowed us to compare different scenarios of symmetric vs. asymmetric excitability profiles relative to that baseline (cf. [20], Fig. 1 for the same rationale for the case of sensorimotor mu-alpha). The rationale is that for a symmetric phasic modulation of corticospinal excitability by the sleep spindle, one would expect balanced amounts of MEP amplitude increases (facilitation) and decreases (inhibition) during the various phases relative to the spindle-free baseline, while an asymmetric phasic modulation would show either more pronounced increases or decreases relative to the spindle-free baseline. The cortical excitability profile we observed for sleep spindles showed a very clear pattern of "asymmetric pulsed inhibition", with a brief pulse of phasic inhibition relative to baseline only occurring during the falling flank of the oscillation and no phasic facilitation occurring at any other phase.

2. Materials and methods

2.1. Subjects

Twenty (N = 20) healthy, right-handed volunteers (12 females; mean age, 23; range, 18–42 years), who were free of medication, had no history of neurological or psychiatric disease, nor any contraindication to TMS [23], participated after providing written informed consent. They were not permitted to consume alcohol or caffeine on the day of the experiment, and they were required to be awake for at least 8 h prior to the experiment to maintain moderate sleep pressure. The study protocol followed the Declaration of Helsinki and was approved by the local ethics committee of the Landesärztekammer Rheinland-Pfalz. Subjects were recruited based on the following inclusion criteria: (1) ability to sleep on their back in supine position for at least an hour without strong snoring (head movements) under the inconvenient experimental conditions; and (2) the presence of a TMS motor hotspot for evoking consistent MEPs of sufficient amplitude (with scalp-cortex distance increased by the EEG cap, reduced stimulator output due to the extra-long coil cable, and the know decrease in MEP amplitudes during sleep) in either the right first dorsal interosseous (FDI) or abductor pollicis brevis (APB) hand muscles. In total, 20 of 31 screened subjects met these criteria, were recruited, and completed the study.

2.2. Experimental design & general procedure

Subjects participated in two nocturnal nap sessions, the adaptation session and the experimental session, which included several preparatory measures as well as the main experiment. Preparatory measures during both sessions (see below for details) included: placement of EEG, polysomnography (PSG), and hand muscle electromyography (EMG)

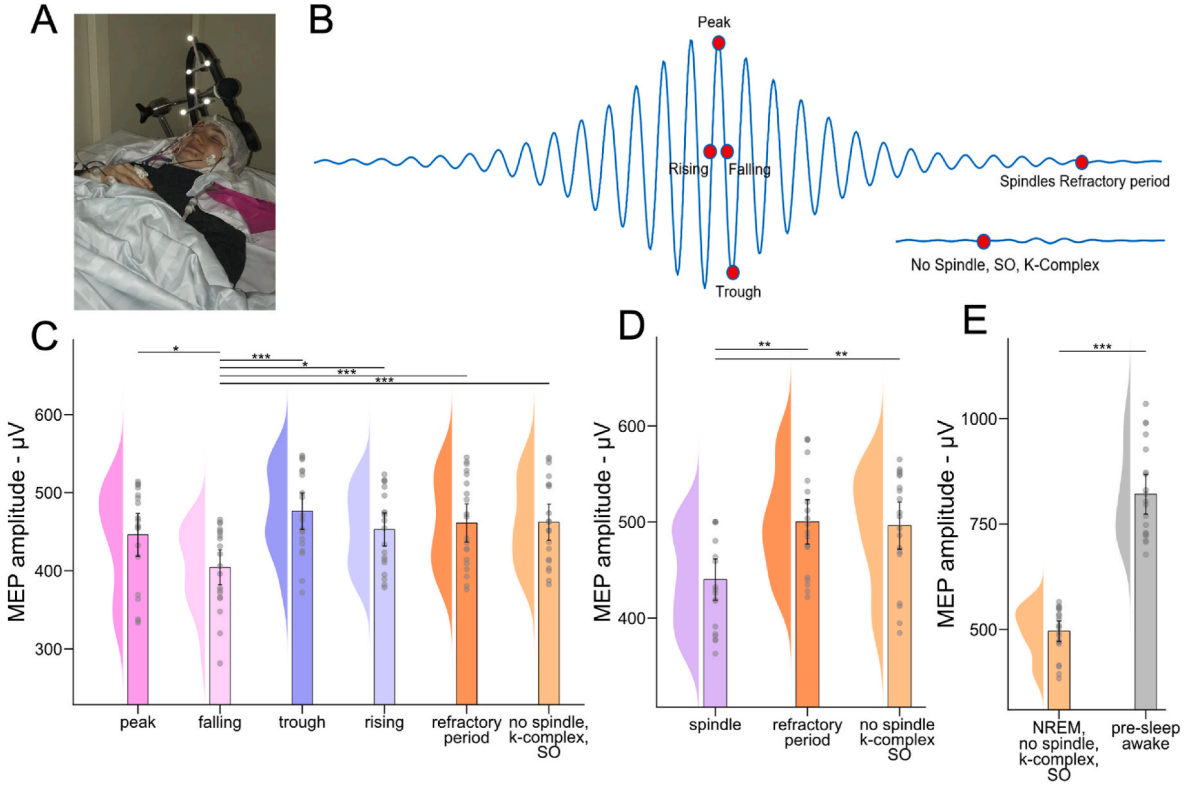

Fig. 1. Real-time EEG spindle phase-triggered TMS. (A) Experimental setup. **(B)** Four distinct phases of the spindle oscillation (trough, rising flank, peak, falling flank) were targeted by single-pulse TMS and compared to spindle- and SO-free intervals and immediately following (post) sleep spindles during refractory period. Significance of post hoc comparisons is indicated as follows: *p < 0.05; **p < 0.01; ***p < 0.001. **(C)** During spindles, MEP amplitudes revealed a rhythmic inhibition of motor corticospinal excitability only at the falling flank. **(D)** Averaged across all spindle phases, the MEP amplitude is still smaller than during spindle-free and spindle-refractory periods. **(E)** During spindle-free baseline NREM periods, MEP amplitude is reduced relative to pre-sleep wakefulness.

electrodes, arrangements for TMS neuronavigation, motor hotspot search, automated determination of resting motor threshold (RMT), and MEP measurements during wakefulness pre-sleep. Participants arrived in the laboratory after at least 8 h of wakefulness during both sessions (Time of arrival (hours - HH), Mean: 19, SD: 04, Range: 14–02). After pre-sleep TMS measurements, they were allowed to fall asleep, sleep for the first few sleep cycles, and then leave the laboratory. Subjects slept in a soundproof and electromagnetically shielded sleeping cabin (Desone, Germany) in a wooden bed on a comfortable mattress, lying on their back in supine position. They were covered with a blanket and had their heads supported by a vacuum cushion. Single-pulse TMS was delivered to the left M1 hand area during the experimental nap session to assess corticospinal excitability. TMS was automatically triggered in real-time (see below for details) to target six different NREM sleep periods: four different phase angles during sleep spindles, i.e., either (1) the peak (0°), (2) the falling flank (90°), (3) the trough (180°), (4) the rising flank (270°), (5) the spindle refractory period (i.e., 1.5 s after the spindle center), or (6) desynchronized periods of NREM sleep where spindles, SOs, or K-complexes were absent (collectively referred as spindle-free condition) (Fig. 1B). The order of these six different experimental conditions was pseudo-randomized across trials to avoid any systematic carry-over effects between conditions.

2.3. EEG, PSG & EMG recordings

64-channel EEG was recorded using a textile EEG cap with extra-flat TMS-compatible sintered Ag/AgCl electrodes according to the 10-10 EE G system and additionally both mastoids, with FCz as recording reference and POz as Ground (Multitrodes-TMS, EasyCap; for a complete list of all electrode positions see Supplementary Material A1). For PSG, EMG at the chin, and the vertical and horizontal electrooculogram (VEOG and HEOG) were recorded using bipolar electrode montages. Surface EMG was recorded with disposable gel electrodes from the right FDI, APB, and ADM muscles in a belly-tendon montage. EEG, PSG, and EMG were digitized in DC mode at 5-kHz sampling rate and with 1250-Hz anti-aliasing low-pass filter, using a TMS-compatible 24-bit amplifier (NeurOne Tesla with Digital-Out Option, Bittium, Finland) connected to an 8-V battery.

2.4. TMS

TMS was applied to the left M1 hand region via figure-of-eight C-B60 coil with an outer diameter of 75 mm connected to a MagPro-X100 stimulator (MagVenture, Denmark). The coil was placed on the head from anteromedial (coil handle) to posterolateral (coil head), and a biphasic pulse with a reversed current direction induced posterolateral-to-anteromedial current in brain tissue for the second, more effective, half-wave. This nontraditional TMS coil positioning, while still producing the standard posterior-to-anterior current flow in the brain due to the reversed current direction of the source, was specifically chosen to accommodate sleeping in the supine position. The MagVenture FlexArm® attached to the base of the wooden bed in the sleep lab held the TMS coil. The coil position that produced consistent MEPs in the right FDI hand muscle (i.e., the 'hotspot') was identified and saved using MR-template-based frameless stereotactic neuronavigation (Localite, Germany). If a consistent TMS hotspot of the right FDI hand muscle could not be established, the TMS hotspot search was then performed for the right APB hand muscle. Participants without consistent MEPs in either muscle were excluded from the study to ensure consistent measurements across subjects. As a result, the right FDI was selected for 16 participants, while the right APB was used for 4 participants only. The BEST toolbox [24] was used to search the motor hotspot and estimate the resting motor threshold (RMT) using an automated closed-loop staircasing procedure. Target stimulation intensity was 130 %RMT (pre-sleep) or 100 %MSO (whichever was lower), resulting in average stimulation intensities of 128 %RMT (SD: 3 %RMT) or 95 %MSO (SD: 5%MSO), respectively. These comparably high intensities were chosen to ensure sufficiently large MEPs during the main experiment despite the known general suppression of MEPs during sleep [21,25–27] as well as the reduced coil output due to the 2m cable extension by which the coil was connected through a shielded cable guide to the stimulator outside the cabin. To avoid TMS discharge sound ("TMS click") related sleep arousals, subjects wore in-ear headphones that delivered a continuous TMS-masking noise generated by the TAAC toolbox [28].

The inter-trial interval (ITI) between consecutive single TMS pulses was designed to range from ~3 to ~7 s, independent of sleep spindle occurrence (see Results for details). Before the start of the experiment, the BEST toolbox generated a trial vector with pseudorandomized experimental conditions (i.e., concatenating "blocks" each of which contained all six conditions in randomized order, ensuring that each condition could occur no more than twice in direct succession), which was then "opportunistically" updated in real-time based on the number of ongoing spindle events in each set of six experimental conditions. The opportunistic strategy in the BEST toolbox was designed to operate in a way that if a planned condition was unavailable, but any of the next 5 planned conditions became possible, the BEST toolbox would trigger for that next possible condition and replace it in the sequence with the currently planned one. This ensured efficient use of available spindle events. In cases where none of the 6 consecutively planned conditions in a block occurred and the maximum ITI of 7 s was reached, the BEST toolbox would trigger a dummy pulse regardless of the planned condition. This approach allowed for flexible adaptation to the unpredictable nature of spindle events while maintaining a quasi-continuous sequence of stimulations within the specified ITI range that would prevent extreme ITI durations from influencing and confounding MEP amplitudes [29].

2.5. Real-time EEG-TMS

The Real-Time Spindle Detector (RTSD) was used to perform real-time EEG analysis to detect sleep spindles and their instantaneous oscillatory phases, as previously described in detail [22]. In summary, EEG data was streamed in real-time to the bossdevice (sync2brain, Germany) that was controlled by the BEST toolbox [24]. To detect centro-parietal spindles and their instantaneous oscillatory phases, a two-channel based spatial filter (bipolar montage) from EEG electrodes C3 and M2 (right mastoid) was used to extract the signal from the left sensorimotor cortex. This montage choice was based on several considerations: (1) the effectiveness of the C3-M2 montage for detecting MEP modulations was shown in previous work on SO-triggered TMS [21]; (2) the validation of our real-time spindle detection algorithm against established offline detection algorithms also confirmed the reliability of the C3-M2 montage for detecting spindles in the left sensorimotor cortex [22]; (3) and although the Hjorth montage is commonly used in real-time EEG-TMS studies of mu-alpha rhythm [19,20], a bipolar montage is considered more suitable for largely synchronized oscillations like sleep spindles, as in such cases the Hjorth montage strongly reduces the signal-to-noise ratio (SNR) by subtracting signals from neighboring electrodes that capture the same oscillatory activity.

EEG recorded during the adaptation nap from each subject was analyzed using YASA [30], i.e., an offline spindle detection software, to obtain the individual spindle band frequency and spindle frequency band (sigma) root mean square (RMS) power threshold required by RTSD for the experimental session, during which instantaneous oscillatory phase was estimated in real-time using the previously published *phastimate* algorithm [31]. The RTSD [22] operates by analyzing 520 ms segments of EEG montage every 10 ms, with a 98 % overlap between consecutive windows. It employs two-pass FIR filters to create a broadband signal (EEG_{bb}) using a 1–30 Hz passband, and a sigma band signal (EEG_{σ}) using a passband centered on the individual's spindle peak frequency ± 2 Hz. Four high-level signals are then derived: EEG_{σ} RMS

power, EEG_{σ} relative power, EEG_{σ} x EEG_{bb} correlation and EEG_{bb} instantaneous frequency. Spindles are detected when at least three of four derived signals exceed individualized thresholds (based on prior baseline sleep data), while also meeting specific duration criteria.

Real-time detection of SOs was merely done to target the spindle- and SO-free baseline NREM epochs conditions and was also performed in the bossdevice. The spatially filtered (i.e. re-referenced) C3-M2 EEG signal was bandpass filtered using two-pass, zero-phase, non-causal finite impulse response (FIR) filter (0.3–1.5 Hz bandpass; Hamming window passband ripple: 0.0194 with 53 dB stopband attenuation; Lower transition bandwidth: 0.20 Hz at −6 dB; Upper transition bandwidth: 1.6 Hz at −6 dB; Filter order: 500). SOs were detected when the bandpass signal exceeded the threshold of mean ± 2 times its standard deviation and the time interval between two subsequent zero crossings in opposite directions was between 0.1 and 1.5 s. While this approach diverges from standard offline methods that typically define SO duration as the full period between positive-to-negative zero crossings, it enabled earlier detection within each potential SO cycle, crucial for precisely timing our designed experimental conditions. YASA was used to extract the individual SO amplitude threshold from the adaptation nap data. Note that this comparably crude SO detection merely served to determine SO-free intervals in real-time and not to perform a detailed SO detection and characterization.

During the experimental sessions, PSG was monitored online to visually score the sleep stages using standard guidelines of the American Academy of Sleep Medicine (AASM) to manually start the real-time EEG triggered TMS at the start of NREM sleep stage 2. TMS intensity was gradually increased to ensure that the subject was not awakened by the sudden delivery of pulses. The total number of ramping pulses varied across subjects, ranging from 12 to 40 trials. All trials collected during the ramping process were discarded later.

2.6. Offline EEG analysis

Standard guidelines of AASM were used to visually score sleep stages using electrode C3 (0.5–40 Hz bandpass filtered) after excluding periods with TMS pulse artifacts and TMS-evoked K-complexes. Unless stated otherwise, all offline analyses were performed using the MNE-Python package [32] and FieldTrip toolbox [33]. EEG analyses were performed post-hoc to distinguish spindles co-occurring with SO from isolated spindles, to validate the performance of real-time EEG analyses, and to calculate the morphological parameters of detected spindles for trial-by-trial correlations with MEP amplitude. EEG data were segmented (−2.5 to −0.004 s relative to TMS), baseline corrected (−0.504 to −0.004 s, avoiding the TMS pulse artifact), and re-referenced to the common average of all EEG electrodes. A virtual channel representing the left sensorimotor cortex signal [C3 - M2 (right mastoid)] was added. EEG data prior to the TMS pulse (−1.5004 to −0.004 s) in the preprocessed EEG segments were further analyzed for offline detection of spindles co-occurring with SO using the slow-wave detection algorithm implemented in YASA [30] based on [34,35]. All detected spindles that co-occurred with SOs were removed from further analysis as the trial count was insufficient (Mean: 37; SD: 8) to make a reliable comparison of isolated spindle conditions to those that co-occurred with SO.

The Pre-TMS EEG data were then further analyzed to verify that TMS was accurately delivered during the intended EEG-defined conditions. To demonstrate frequency-specificity to the targeted sleep spindles, time-frequency representations (TFR) were calculated for the pre-TMS period, for a period ranging from −1.5 to 1 s, with the post-TMS period replaced by zeros to prevent any TMS-related responses and artifacts from corrupting power estimates in the pre-TMS period. We applied the multitapers convolution method with a dynamic window length of 5 cycles of a given frequency, a step size of 20 ms, and a frequency resolution of 0.5 Hz, with a range of 1–35 Hz baseline corrected from [−0.5 to −0.4] s using a relative percentage change method. For each time-frequency point, we calculated the mean power during the baseline period ([−0.5 to −0.4] s) and then computed the percent change using the formula ((power - mean_baseline_power)/mean_baseline_power) × 100 %. This expresses each power value as a percentage change relative to the baseline period. To illustrate the topographical specificity of the targeted sleep spindle power, the topographical distribution of baseline corrected pre-TMS spindle power values was plotted per condition. Pre-TMS time-series were averaged across trials per subject and condition to demonstrate phase-specificity. Because the instantaneous phase of TMS delivery could not be calculated directly for the time point of stimulation due to signal corruption caused by TMS-evoked potentials and -related artifacts, it was estimated for each trial at one individual spindle cycle earlier [20]. It is worth noting that the phase estimates do not reveal any hardware or software-related signal processing delays because they were compensated for prior to forecasting the instantaneous oscillatory phase in each trial.

For each spindle trial, we analyzed the pre-TMS data (−1.004 to −0.004 s) to calculate six key morphological parameters in the following order: (1) instantaneous voltage at TMS delivery, (2) sigma power, (3) spindle frequency, (4) 1/f aperiodic power level, (5) spindle duration, and (6) maximum voltage (Fig. S1, Table S1). The instantaneous voltage captures the absolute value of the amplitude envelope of the spindle at the exact moment of TMS delivery (−0.004 s), derived from the sigma band power calculation as previously described in RTSD [22]. The sigma power, calculated as the mean power across the 12–15 Hz band, quantifies the overall strength of spindle activity. The power spectrum obtained from the fast Fourier transform (FFT) of a 1 s pre-TMS data was used to calculate frequency. Specifically, we defined spindle frequency as the peak frequency within the 12–15 Hz sigma band. To quantify the background neural activity separate from the spindle oscillation, we calculated the 1/f levels, i.e., average power of the aperiodic signal across the sigma frequency band, using the “fitting oscillations & one-over f (FOOOF)" tool [36]. FOOOF was configured with a frequency range of 1–40 Hz, a peak width limit of 0.5–4 Hz, a minimum peak height threshold of 0.05, and the knee parameter enabled to capture low-frequency curvature in the aperiodic component. The aperiodic mode was set to “fixed" to ensure robust characterization of the slope across the sigma frequency band. The highest aperiodic power within the sigma frequency band (i.e., the peak value of the fitted aperiodic component in the 12–15 Hz range) was used as the 1/f level of spindle for each trial. The spindle duration measures how long the spindle had been active before TMS delivery, calculated as the difference between time at TMS delivery and its nearest possible sample when the sigma RMS power was found to be less than the “entry RMS threshold" of mean + 1.15 SDs (standard deviation) of the baseline RMS power, i.e., adaptation nap sigma RMS power. The maximum voltage represents the highest voltage reached by the spindle during its occurrence pre-TMS, derived using the same sigma band power calculation method as the instantaneous voltage.

Preprocessed EEG data segments were averaged per condition (spindle-peak, spindle-falling flank, spindle-trough, spindle-rising flank, spindle-refractory period, no-spindle/SO/K-complex) time-locked to the TMS pulse. Subject-wise averages were then aggregated to obtain grand averages for each condition.

2.7. Offline EMG analysis

EMG data were analyzed using BEST and FieldTrip toolboxes [24,33]. In summary, raw EMG data was epoch from [−50 to +100] ms around the TMS pulse. To rectify the DC offset, the data were demeaned relative to a pre-TMS data window of [−50−5] ms. The amplitude of the MEP was computed by measuring the peak-to-peak value within a constant window of [15 50] ms after TMS pulse (Fig. 1). In addition to the raw MEP amplitude results shown in Fig. 1, we also calculated normalized MEP amplitudes using a running window approach, which is largely equivalent to the normalization per discrete experimental block as routinely reported in real-time phase-/amplitude-triggered TMS

studies during wakefulness [19,20,37]. Specifically, we expressed each MEP peak-to-peak amplitude as a percent change relative to the mean of its surrounding 120 trials (across all conditions, centered on the current trial). This running window normalization was applied to account for slow drifts in corticospinal excitability. The normalized amplitudes were then averaged for each phase condition. However, given the clarity of the raw MEP results in this study, normalized amplitudes were not essential and are thus provided only in Supplementary Fig. S2 for reference.

2.8. Statistics

The independent variable was the targeted EEG-defined NREM sleep state, which was realized as a within-subject factor with the following six levels: spindle trough, spindle rising flank, spindle peak, spindle falling flank, spindle refractory period, and periods with no spindle, SO, or K-complex. The main dependent variable was corticospinal excitability as indexed by MEP amplitude. One-way rmANOVAs were conducted with post-hoc paired *t*-test where applicable. For the post-hoc analyses, p-values were adjusted (p_{adj}) using the Bonferroni-Holm method to control for alpha error accumulation across the 15 possible pairwise comparisons between the six conditions. Statistical analyses were conducted using Python 3.11 (scipy.stats functions f_oneway and ttest_rel; statsmodels. stats.multitest function multipletests for Bonferroni-Holm correction). Effect sizes for ANOVA (F-values) and *t* tests (Cohen's d_{av}, based on the averaged SD) are provided (Lakens, 2013). To assess phase angle distributions, Rayleigh's test from the SciPy library [38] was used to evaluate general deviations from uniformity. Additionally, directed deviations toward the targeted phase angle were assessed using the V-test from the CircStat toolbox [39]. The electrode-wise MEP-spindle single trial correlations in supplementary analysis (Fig. S1) were tested for significance using cluster-based permutation tests with correction for multiple comparisons [33]. Correlational analyses were performed on each channel to test for a linear relationship between trial-by-trial variations in normalized MEP amplitudes and spindle morphological parameters at the time of stimulation. Correlation coefficients were calculated separately for all spindle phase-triggered conditions in every subject, Fischer z-transformed, and were then tested channel-wise on the group level using two-sided paired *t*-test.

3. Results

During the experimental nap, where TMS was administered, subjects slept for an average of 97.3 ± 21 min. Average spindle density during the experimental nap was 4.8 ± 0.4 spindles per minute NREM sleep, and subjects received a total of 796 ± 84 TMS pulses, including dummy trials. On average, 86 ± 15 trials were acquired per experimental condition (spindle-peak, spindle-falling flank, spindle-trough, spindle-rising flank, spindle-refractory period, spindle-free), resulting in 74 ± 5 trials included in the analyses after exclusion of trials where spindles occurred concurrently with an SO. The median inter-trial interval between two consecutive TMS trials was 4.7 ± 1.2 s, with no statistical difference between conditions (paired *t*-test $p > 0.7$).

3.1. Sleep spindles phasically inhibit MEP corticospinal excitability

MEP amplitudes were modulated by sleep spindle phases ($F_{(5,95)} = 3.98$, $p = 0.002$; Fig. 1C). MEPs were smaller during the sleep spindle falling flank than during any other condition (falling vs trough: $t_{19} = 4.28$, $p = 0.0004$ ($p_{adj} = 0.003$*), Cohen's *d*av = 1.35; falling vs refractory: $t_{19} = 3.93$, $p = 0.0009$ ($p_{adj} = 0.004$*), Cohen's *d*av = 1.04; falling vs spindle-free: $t_{19} = 3.90$, $p = 0.0009$ ($p_{adj} = 0.004$*), Cohen's *d*av = 1.09; falling vs rising: $t_{19} = 2.7$, $p = 0.01$ ($p_{ad} = 0.004$), Cohen's *d*av = 0.95; falling vs peak: $t_{19} = 2.3$, $p = 0.03$ ($p_{adj} = 0.005$), Cohen's *d*av = 0.51). This means that corticospinal excitability was rhythmically suppressed during the falling flanks of the sleep spindle oscillation (by 12 % on average) while remaining at levels comparable to the spindle-free baseline NREM periods during the spindle troughs, rising flanks, peaks, and refractory post-spindle periods. Sleep spindle phases also modulated normalized MEP amplitudes (Fig. S2).

When ignoring spindle phase and averaging across all spindle conditions, MEP amplitude was still smaller than during the absence of spindle/SO/K-complex (spindle-free condition) in NREM sleep ($t_{19} = 3.30$, $p = 0.004$, Cohen's *d*av = 1.04; Fig. 1D) and spindle refractory period ($t_{19} = 3.22$, $p = 0.004$, Cohen's *d*av = 1.15; Fig. 1D). A comparison of the MEPs measured during the spindle refractory period and the baseline spindle-free oscillatory state in NREM sleep revealed no statistically significant difference ($p > 0.8$). By comparing the pre-sleep wakefulness cortical excitability with NREM spindle-free periods we found the MEP amplitude to be generally decreased (by 39 % on average) during NREM sleep ($t_{19} = 10.3$, $p < 2e\text{-}9$, Cohen's *d*av = 3.87; Fig. 1E).

3.2. Real-time EEG-triggered TMS successfully targeted sleep spindle and phases

The additional offline analyses of pre-TMS EEG confirmed that TMS was delivered at the intended EEG-defined brain-states and that no systematic confounds occurred (Fig. 2) as evident by time-frequency responses (Fig. 2A), topographical distributions of sleep spindle power (Fig. 2B), estimated spindle phases at the time of actual TMS pulse delivery (Fig. 2C), and time-locked averaged EEG signals (Fig. 2D). According to these analyses, sleep spindles, spindle phases, and desynchronized oscillatory states were consistently targeted across subjects (mean circular standard deviation of 51° for all sleep spindle phase targeted conditions; ~10 ms for an averaged 13 Hz sleep spindle), and adjacent frequencies or oscillatory activity from other sources, e.g., SO or broad frequency band noise did not confound the results. Rayleigh's test confirmed a significant deviation of the detected sleep spindle phase angles from a uniform distribution (peak: $R = 0.78$, $p = 0.03$; falling: $R = 0.73$, $p = 0.04$; trough: $R = 0.72$, $p = 0.04$; rising: $R = 0.72$, $p = 0.04$). Additionally, V-tests indicated a significant directed deviation towards the targeted phase angle (peak: $V = 0.91$, $p = 0.02$; falling: $V = 0\,0.83$, $p = 0.03$; trough: $V = 0.84$, $p = 0.03$; rising: $V = 0.86$, $p = 0.03$).

3.3. No effect of spindle morphology on MEP corticospinal excitability

Trial-by-trial variations in spindle instantaneous amplitude at the time of TMS, sigma oscillatory power, 1/f level, spindle peak frequency, duration of spindle at the time of TMS, and maximum instantaneous spindle amplitude did not correlate with trial-by-trial variations in MEP amplitude (Fig. S1). The correlations were extremely weak, statistically insignificant (all $p > 0.05$) with r-values ranging from −0.1 to 0.1, and topographies did not reveal any consistent pattern across indices.

4. Discussion

We report first empirical evidence that the sleep spindle reflects asymmetrical pulsed inhibition of corticospinal excitability. MEP amplitudes were inhibited during the falling flank of the spindle oscillation, relative to the desynchronized baseline NREM sleep state, when spindles/SOs/K-complexes were absent (spindle-free), spindle refractory periods, as well as spindle troughs, rising flanks, and peaks. Our findings suggests that sleep spindles do not simply exert a tonic inhibition of corticospinal excitability compared to spindle-free or spindle refractory periods, but a rhythmic suppression at a very limited part of the spindle oscillatory cycle, with no effect during the remaining phases. This study further confirms previous reports that corticospinal excitability is markedly suppressed during NREM sleep, as evidenced by lower MEP amplitudes compared to pre-sleep wakefulness. Unlike

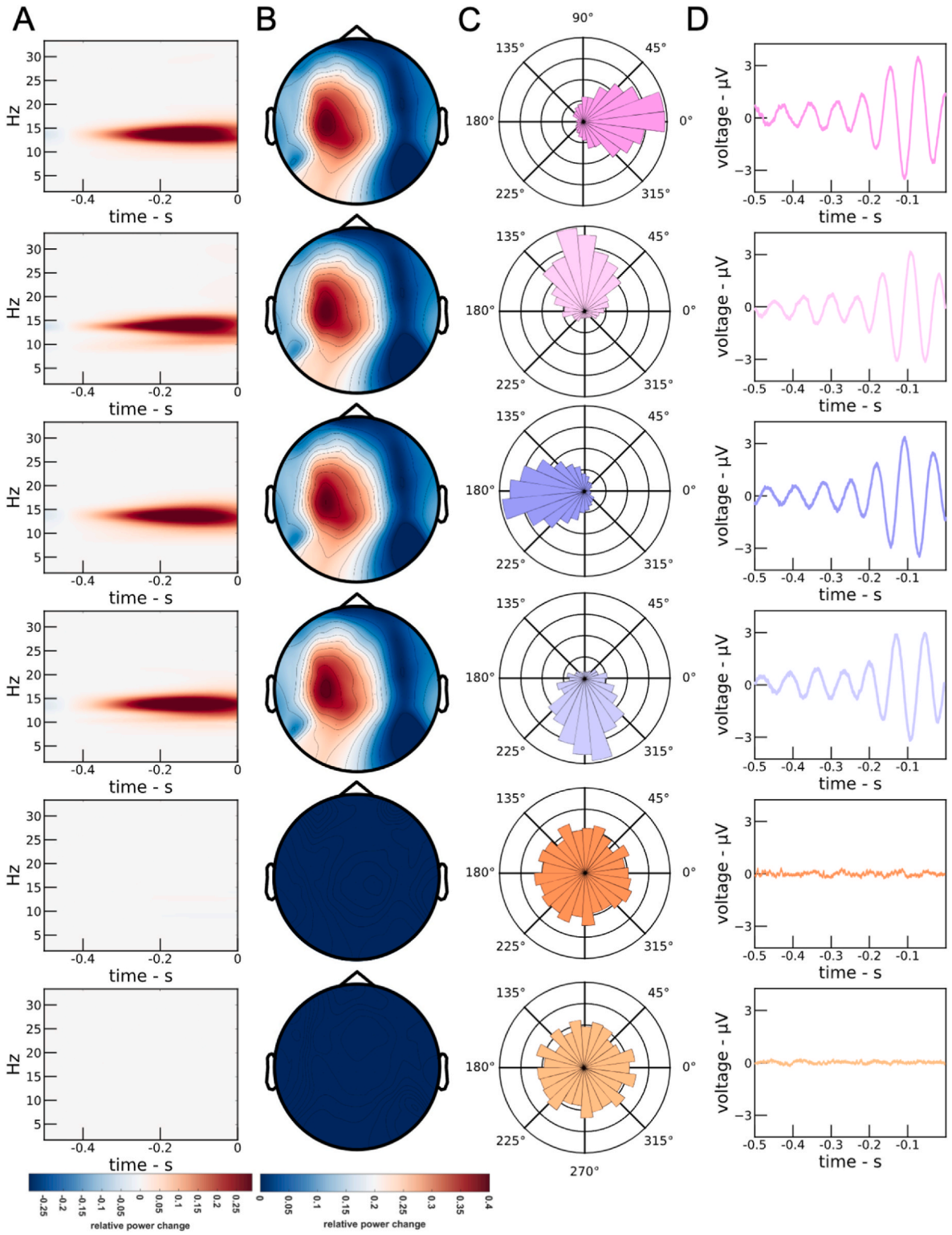

Fig. 2. Sleep spindles and instantaneous phases were successfully targeted. (A) TFRs of oscillatory power in the C3-right mastoid signal prior to TMS (delivered at time point 0 ms). **(B)** Topographical maps of pre-TMS [-0.3 to −0.1s] spindle power. Note that the scaling of the relative power change values in TFRs (A) and topographical maps (B) is consistent across all conditions and therefore appears uniform in the absence of spindles. **(C)** Phase histogram illustrating instantaneous phases in the C3-right mastoid signal one spindle cycle before TMS delivery. **(D)** Averaged time-locked C3-right mastoid signal relative to delivery of TMS (at 0 ms) highlighting sigma (12–15 Hz) activity in spindle conditions. The color code in this figure is consistent with that used in Fig. 1 for ease of comparison: dark pink (peak), light pink (falling phase), dark purple (trough), light purple (rising phase), orange (sleep spindle refractory period), and beige (NREM baseline without sleep spindles, SOs, or K-complexes).

established for SOs in a previous study [21], there was no evidence linking corticospinal excitability (MEP amplitude) to spindle instantaneous amplitude nor any other morphological characteristic such as sigma oscillatory power, 1/f level, peak spindle frequency, spindle duration, or maximum instantaneous spindle amplitude.

4.1. Sleep spindle phase-dependent rhythmic inhibition of corticospinal excitability

Sleep spindle falling flanks, but not any of the other tested phase angles (troughs, rising flanks, and peaks), were associated with inhibition of corticospinal excitability relative to the spindle-free baseline NREM state, while no relative facilitation was observed during any of the experimental conditions. To date, no comparable data exists that provide insights into the phase-resolved excitability profile of sleep spindles, neither from human nor animal work. Therefore, we can only compare our findings to those of previous studies on other neuronal oscillations and their phase-dependent modulation of M1 corticospinal excitability. During NREM sleep, the SO up-state was shown to be associated with larger excitability than the SO down-state [21]. Unfortunately, no MEPs were recorded during SO-free NREM sleep as baseline, so that a potential asymmetry and directionality of the SO phase-dependent modulatory effect could not be investigated. Also, rising and falling flanks of the SO were not probed, so that the actual excitability minima and maxima of the SO remain yet to be determined. During wakefulness, corticospinal excitability was found to be larger during the trough than peak of the sensorimotor mu-alpha (~8–14 Hz) rhythm [19,20,40,41], later also qualified as asymmetric pulsed facilitation relative to a desynchronized mu-alpha-free background state [20]. A recent study replicated mu-alpha phase-dependent effects on M1 cortical excitability [42]. Furthermore, also studies using post-hoc sorting of trials according to mu-alpha phase revealed a similar phasic modulation of corticospinal excitability [43,44], while further refining the excitability maximum from trough to early rising phase of the mu-alpha cycle [45]. Similarly, future studies may use either spindle-triggered random phase MEP measurements or phase-triggered MEPs at higher phase resolution to further narrow down the specific excitability minima/maxima for spindles. In any case, our findings appear to be in good agreement with the notion of an oscillatory phase-dependent modulation of corticospinal excitability in the human M1.

A direct comparison of the phasic excitability profiles of spindle and mu-alpha oscillations, which cover roughly the same frequency space during NREM sleep and wakefulness, respectively, and both show a topographical maximum over central sensorimotor regions, reveals interesting differences and similarities. In fact, the relative phase-excitability relationship appears highly similar for the two oscillations, while the asymmetry of the phasic modulation appears to be of opposite direction, resembling pulsed facilitation for mu-alpha versus pulsed inhibition for spindles. Whether this is due to their different neurophysiological mechanisms of generation or different excitability levels of the respective baseline periods during wakefulness and sleep, remains to be determined. Notably, both spindles and mu-alpha show a very different phase-excitability relationship than SOs, for which the excitability was larger during the surface EEG peak than trough, here reflecting the depolarized up-state and hyperpolarized down-state, respectively.

4.2. Spindle refractoriness has no effect on corticospinal excitability

Spindles are less likely to occur up to 3 s after the occurrence of the previous spindle [46], indicating a refractory period during which the neurophysiological mechanisms necessary for spindle generation may be dormant [6,9,47]. Prior research even suggested that spindle refractoriness may be crucial for memory reactivation [46], as targeted memory reactivation had stronger effects on memory retention if applied after as compared to during the spindle refractory period [46]. However, this refractory period does not seem to be related to a transient reduction in cortical excitability but rather excitability changes in thalamic neurons, as we did not observe a difference in MEP amplitudes between random periods of desynchronized baseline NREM spindle-free periods and periods of spindle refractoriness.

4.3. Sleep-dependent changes in corticospinal excitability

Our findings also corroborate the notion of a general NREM sleep-dependent suppression of corticospinal excitability, as reported by previous TMS studies during sleep. MEP amplitudes were generally found to be decreased during NREM sleep compared to pre-sleep wakefulness [21,25–27]. This general transition from pre-sleep wakefulness to deep sleep has been linked to suppression of excitability at the spinal level, possibly also related to the characteristic neuromuscular blockade during NREM - and in particular REM sleep [26] - but increased paired-pulse short latency intracortical inhibition suggests a cortical contribution as well [25,27].

4.4. Relevance of spindle morphology

We found no correlation between sleep spindle instantaneous amplitude and MEP amplitude ($p > 0.05$). This result is not in line with previous studies, as a significant trial-by-trial correlation between the actual oscillatory SO amplitude and the evoked MEP amplitude was observed during sleep [21], and event-wise variations in spindle amplitude also predicted spindle-related BOLD response amplitude during concurrent EEG-fMRI measurements [1]. Additionally, real-time EEG power triggered TMS also demonstrated that corticospinal excitability increased with the power of the sensorimotor mu-alpha rhythm [37]. Further analysis also revealed no relationship between MEP amplitude and any of the other calculated spindle morphological parameters including sigma power, frequency, duration, 1/f level, or maximum spindle amplitude ($p > 0.05$). We assumed that MEP amplitudes would, at least during the spindle falling-flank phase angle experimental condition, correlate with the trial-by-trial variation in spindle instantaneous amplitude or other morphological parameters because MEPs in this condition were significantly suppressed compared to all other conditions. It is possible that the amplitude threshold used for spindle detection did reduce their variance to a degree that the remaining spindle amplitude differences were too small to impact MEP amplitude.

4.5. Potential mechanisms mediating sleep spindle phase-dependent inhibition of corticospinal excitability

Sleep spindles emerge from complex interactions within thalamocortical circuits. In the thalamus, GABA-ergic neurons in the reticular nucleus (TRN) interact with glutamatergic thalamocortical (TC) relay neurons to generate the characteristic spindle pattern. These TC neurons project to the neocortex, while receiving feedback from cortical neurons, allowing for bidirectional regulation of spindle dynamics [5,48].

Recent research in rodents has provided detailed insights into the cellular mechanisms of spindle generation and their relation to other sleep oscillations. Using calcium imaging and Local Field Potential recordings, studies have demonstrated the crucial role of parvalbumin-positive (PV+) GABAergic inhibitory interneurons in both thalamic and cortical circuits during spindles [49–51]. In the neocortex, spindles are associated with distinct activation patterns across different neuron types. While both excitatory pyramidal (PYR) cells and PV + interneurons show increased firing rates during spindles, PV + activation is particularly pronounced [15–17]. In contrast, somatostatin-positive (SOM+) interneurons decrease their activity [15,16], and vasoactive intestinal polypeptide (VIP)-positive interneurons maintain stable firing rates [15].

This orchestrated activity of different interneuron types appears

particularly important when spindles occur during slow oscillation (SO) up-states. During these nested events, PV + activity is enhanced while SOM + activity is reduced, leading to a threefold increase in PYR cell activity compared to isolated events [16]. This specific balance of inhibitory inputs may facilitate synaptic plasticity during memory consolidation, as reduced dendritic inhibition (via decreased SOM + activity) enables strong postsynaptic activation while enhanced perisomatic inhibition (via increased PV + activity) controls output firing [4,16].

Human recordings have corroborated these findings, showing increased spiking of both pyramidal cells and interneurons during spindles, particularly when nested in SO up-states [52]. Importantly, these neurons show phase-locking to the spindle oscillation, suggesting temporal coordination of neural activity. This phasic modulation extends to faster oscillations, with both cortical gamma power and hippocampal ripples showing phase-coupling to spindles [53–56]. However, it is crucial to note that the specific phase relationships observed in surface EEG are heavily dependent on recording montage and reference placement, making direct interpretations of particular phases (such as the falling flank) challenging.

Our observed phase-dependent suppression of corticospinal excitability, combined with the known increase in PV + interneuron activity during spindles, suggests a mechanism of rhythmic inhibition rather than facilitation. Future studies using paired-pulse TMS protocols could directly test this hypothesis by measuring GABA-A-receptor mediated inhibition across spindle phases, similar to investigations of the sensorimotor mu-alpha rhythm [20].

4.6. A route towards spindle phase-dependent plasticity and probing their causal role in sleep-dependent memory consolidation

Beside advancing our fundamental understanding of spindle physiology, the unique experimental setup we established and the resulting characterization of a clear spindle phase-excitability relationship have also direct implications for the development of novel EEG-triggered TMS protocols to investigate both spindle phase-dependent plasticity and the causal role of spindles in memory reactivation and consolidation.

Spindles have long been associated with windows of synaptic plasticity during sleep. Stimulation of cortical pyramidal cells with spindle-like 12–15 Hz pulse sequences promoted Ca^{2+}-dependent long-term potentiation (LTP) of excitatory postsynaptic potentials, suggesting that spindles may also contribute to spike timing-dependent plasticity (STDP) via Ca^{2+} influx into cortical neurons [52,57,58]. The hypothesis of 'phase-dependent plasticity' assumes particularly strong Ca^{2+} influx and associated LTP when spindles are precisely timed to the depolarizing phase of neocortical SOs [3,59] and ripples to the most excitable phase of spindles [55]. An example of phase-dependent plasticity has also been demonstrated in rat hippocampal slices, where bidirectional synaptic plasticity could be induced when administering single bursts of electrical stimulation to opposite phases of the theta oscillation that differed with respect to their associated postsynaptic membrane potential [60]. Phasic excitability modulations during oscillations are thus believed to be a basic requirement for their proposed phase-dependent plasticity mechanism [3], and the same neurophysiological mechanisms underlying EIB fluctuations during spindles and SOs are presumably also responsible for the synaptic rescaling of neocortical synapses as a mechanism of systems memory consolidation during sleep [4,18,61,62].

To tap into the mechanism of phase-dependent plasticity [3], TMS burst need to be delivered repetitively to the most (vs. least) excitable phase of an oscillation, as repeatedly demonstrated for the sensorimotor mu-alpha rhythm during wake, where repeated delivery of 100–200 Hz TMS bursts to M1 during the more excitable trough of the oscillation, as previously determined in a separate experiment [19], produced a lasting long-term potentiation (LTP)-like increase in corticospinal excitability, whereas delivery of the same burst to the less excitable mu-alpha peaks did not, and random phase delivery of 200 Hz burst even caused long-term depression (LTD)-like decreases [19,63,64]. Importantly, identifying phases of "high" vs. "low" excitability is an important prerequisite for subsequently designing effective phase-dependent plasticity protocols [19], and for sleep spindles this information cannot simply be inferred from other neuronal oscillations such as wake mu-alpha [20,65] or sleep SOs [21] since their underlying mechanisms of generation differ fundamentally and so may their respective phase-excitability profiles. The demonstration of a spindle-phase specific excitability profile does therefore not only support the plausibility of phase-dependent plasticity at the level of spindle-ripple coupling but also inform the subsequent design of spindle-targeting TMS protocols aiming for the demonstration of phase-dependent plasticity or the interference with sleep-dependent memory replay.

Based on the observed phase-excitability relationship of spindle oscillations, one may speculate that the repeated application of gamma-/ripple-like TMS bursts during spindles targeting the phase of maximum inhibition (for our EEG montage corresponding to the falling flanks of the oscillation) would cause LTD-like MEP decreases, while targeting the troughs may cause LTP-like increases. The latter assumption would be based on the notion that spindle troughs descriptively showed the largest MEPs (even though not different from baseline or any of the other conditions despite falling flanks) but more importantly that this phase immediately follows the strong suppression during the falling flank and thereby potentially represents a state of release from inhibition (or disinhibition) that may facilitate LTP [66].

It can be suggested that sleep spindle trough (least inhibitory) triggered rTMS may lead to LTP-like effects similar to the previously reported mu-alpha trough triggered (most excitable) rTMS of M1 that lead to LTP-like effects in wakefulness [19]. These mu-alpha dependent LTP-like effects were attributed to the disinhibition potentially associated with the facilitatory effects of motor cortical neurons at the trough following the least facilitatory peaks, given the general relevance of disinhibition for TMS-related LTP-like plasticity [66]. Similar to the recently reported mu-alpha random phase triggered 200 Hz bursts of rTMS over M1 that induce LTD-like effects during wakefulness [64], tonically (i.e., random phase) triggered rTMS during thalamocortical spindle may also result in LTD-like effects on corticospinal excitability. Moreover, repeatedly targeting spindles or even specific spindle phases with TMS may allow researchers to deliberately interfere with processes of memory reactivation and associated synaptic rescaling in the neocortex as part of the hippocampo-neocortical dialogue mediated by SO-Spindle-ripple PAC [2,55,67] and thereby demonstrate the causal role of sleep spindles in systems memory consolidation.

4.7. Limitations

This study is the first one of its kind, using real-time EEG spindle phase-triggered targeting of M1 with TMS during human NREM sleep to provide a phase-resolved characterization of the corticospinal excitability pattern associated with sleep spindles. This demanding methodological setup naturally comes with a number of limitations. Firstly, unlike established offline spindle detection algorithms that can use information of entire spindle waveforms and even entire sleep recordings, the dedicated real-time spindle detection (RTSD) algorithm [24] we used is causal by design to work in real-time, meaning that it can only use the data recorded up to the current point in time. Therefore, spindles can only be detected after they have already emerged to a sufficient extent and meet certain amplitude criteria. They are thus detected and targeted more often in their second half (the waning phase of their amplitude), while their first half (with waxing amplitude) remains largely unstudied. Second, we sampled MEPs from only four spindle phase angles (trough, rising flank, peak, and falling flank), and it is well possible that additional or even stronger modulation occurs during phase angles not sampled in this study. Future studies using spindle event-triggered but phase-random targeting with post hoc phase-sorting

may reveal a more fine-grained resolution of the phasic excitability dynamics, as in [45]. Third, spindles and SOs frequently co-occur in deep NREM sleep [55,68,69], and the precise spindle-SO phase-amplitude coupling has been shown to affect neuronal (co-)firing [52] and the specific pattern of excitatory and inhibitory neuronal involvement [16]. This is thought to play an important role in memory consolidation [59,70,71], likely via the mechanism of phase-dependent plasticity [3]. Comparing phasic corticospinal excitability modulations during isolated spindles with those nested in SO up-states would thus have been highly interesting but was unfortunately not possible due to very little deep NREM sleep in the current study and thus an insufficient number of spindles co-occurring with SOs. Fourth, the observed modulation of corticospinal excitability by spindle phase may be specific to M1 and not translate to other cortical regions and other outcome measures or do so but with shifts in the specific phase angles showing maximal effects, due to the traveling wave like properties of spindles and SOs and the resulting phase differences between cortical regions [35,52]. However, the clear advantage of M1 as a model system is that it allows for an objective assessment of phasic modulations in corticospinal excitability via the well-established MEP, while the assessment of cortical excitability outside M1 is challenging, e.g., using TMS-evoked EEG potentials (TEPs), which require complex experimental controls to deduce meaningful excitability indices, in particular when time-locked to oscillatory phases [72,73].

5. Conclusion

We provide the first in-human demonstration of the feasibility of real-time sleep spindle phase-triggered TMS and of a phasic modulation of corticospinal excitability by the sleep spindle. Our findings are best explained by sleep spindles exerting an asymmetrical “pulsed inhibition” on corticospinal excitability, complementing previous work demonstrating a phasic modulation of corticospinal excitability by the sleep SO [21] as well as asymmetrical “pulsed facilitation” by the sensorimotor mu-alpha rhythm during wakefulness [19,20]. Utilizing this technique, future work should further characterize the excitation-inhibition profile of sleep spindles, investigate their interaction with SOs, and test their role as windows of phase-dependent synaptic plasticity as well as their causal relevance for memory reactivation in the context of systems memory consolidation.

CRediT authorship contribution statement

Umair Hassan: Writing – review & editing, Writing – original draft, Visualization, Validation, Supervision, Software, Resources, Project administration, Methodology, Investigation, Formal analysis, Data curation, Conceptualization. **Prince Okyere:** Writing – review & editing, Resources, Project administration, Formal analysis, Data curation. **Milad Amini Masouleh:** Writing – review & editing, Formal analysis, Data curation. **Christoph Zrenner:** Writing – review & editing, Investigation, Formal analysis. **Ulf Ziemann:** Writing – review & editing, Supervision, Funding acquisition, Formal analysis, Conceptualization. **Til Ole Bergmann:** Writing – review & editing, Visualization, Validation, Supervision, Software, Resources, Project administration, Methodology, Investigation, Funding acquisition, Formal analysis, Data curation, Conceptualization.

Code and data availability

The code and data that support the findings of this study are available from the main author, U.H., upon request.

Competing financial interests

U.H. discloses a prior employment at sync2brain GmbH where he was head of firmware and embedded software engineering team. sync2brain GmbH, Germany, is a start-up spin-off company that commercializes the real-time EEG analysis hardware and software that was used in this study. C.Z. and U.H. disclose a minority interest in sync2brain GmbH (Tübingen, Germany). All other authors declare no competing financial interests.

Declaration of competing interest

U.H. discloses a prior employment at sync2brain GmbH where he was head of firmware and embedded software engineering team. sync2brain GmbH, Germany, is a start-up spin-off company that commercializes the real-time EEG analysis hardware and software that was used in this study. C.Z. and U.H. disclose a minority interest in sync2brain GmbH (Tübingen, Germany). All other authors declare no competing financial interests.

Acknowledgments

T.O.B. received support from funding from the Boehringer Ingelheim Foundation (BIF) and the German Research Foundation (DFG Grant 468645090); C.Z. acknowledges support by an Academic Scholars Award from the Department of Psychiatry, University of Toronto, as well as grant support from the Brain Canada Foundation, the Brain and Behaviour Research Foundation (grant agreement No. 31954), the Canadian Institute for Health Research (grant agreement No. 481302) and the Canada Foundation for Innovation with Co-Financing from the Ontario Research Fund. C.Z. received support from the German Federal Ministry for Economic Affairs and Energy through an EXIST Transfer of Research (grant no. 03EFJBW169); U.Z. received support from the European Research Council (ERC Synergy) under the European Union’s Horizon 2020 research and innovation program (ConnectToBrain; grant agreement No. 810377) and from the German Research Foundation (DFG Grant 468645090).

Appendix A. Supplementary data

Supplementary data to this article can be found online at https://doi.org/10.1016/j.brs.2025.02.015.

References

[1] Bergmann TO, Mölle M, Diedrichs J, Born J, Siebner HR. Sleep spindle-related reactivation of category-specific cortical regions after learning face-scene associations. 2 Neuroimage 2012;59:2733–42.
[2] Diekelmann S, Born J. The memory function of sleep. 2 Nat Rev Neurosci 2010;11:114–26.
[3] Bergmann TO, Born J. Phase-amplitude coupling: a general mechanism for memory processing and synaptic plasticity?. 1 Neuron 2018;97:10–3.
[4] Klinzing JG, Niethard N, Born J. Mechanisms of systems memory consolidation during sleep. 10 Nat Neurosci 2019;22:1598–610.
[5] Fernandez LMJ, Lüthi A. Sleep spindles: mechanisms and functions. 4 Physiol Rev 2020;100:805–68.
[6] Bal T, McCormick DA. What stops synchronized thalamocortical oscillations?. 8 Neuron 1996;17:297–308.
[7] Bonjean M, Baker T, Lemieux M, Timofeev I, Sejnowski T, Bazhenov M. Corticothalamic feedback controls sleep spindle duration in vivo. 6 J Neurosci 2011;31:9124–34.
[8] Destexhe A, Bal T, McCormick DA, Sejnowski TJ. Ionic mechanisms underlying synchronized oscillations and propagating waves in a model of ferret thalamic slices. 9 J Neurophysiol 1996;76:2049–70.
[9] Lüthi A, McCormick DA. Periodicity of thalamic synchronized oscillations: the role of Ca2+-mediated upregulation of ih. 3 Neuron 1998;20:553–63. https://doi.org/10.1016/S0896-6273(00)80994-0.
[10] Lüthi A, McCormick DA. Modulation of a pacemaker current through Ca2+-induced stimulation of cAMP production. 7 Nat Neurosci 1999;2:634–41. https://doi.org/10.1038/10189.
[11] Timofeev I. Contribution of intrinsic and synaptic factors in the desynchronization of thalamic oscillatory activity. 3 Thalamus Relat Syst 2001;1:53–69.
[12] Barthó P, Slézia A, Mátyás F, Faradzs-Zade L, Ulbert I, Harris KD, Acsády L. Ongoing network state controls the length of sleep spindles via inhibitory activity. 6 Neuron 2014;82:1367–79. https://doi.org/10.1016/j.neuron.2014.04.046.

[13] Langdon AJ, Breakspear M, Coombes S. Phase-locked cluster oscillations in periodically forced integrate-and-fire-or-burst neuronal populations. 12 Phys Rev 2012;86:061903.
[14] Rovo Z, Matyas F, Bartho P, Slezia A, Lecci S, Pellegrini C, Astori S, David C, Hangya B, Luthi A, Acsady L. Phasic, nonsynaptic GABA-A receptor-mediated inhibition entrains thalamocortical oscillations. 5 J Neurosci 2014;34:7137–47.
[15] Brécier A, Borel M, Urbain N, Gentet LJ. Vigilance and behavioral state-dependent modulation of cortical neuronal activity throughout the sleep/wake cycle. 6 J Neurosci 2022;42:4852–66. https://doi.org/10.1523/JNEUROSCI.1400-21.2022.
[16] Niethard N, Ngo H-VV, Ehrlich I, Born J. Cortical circuit activity underlying sleep slow oscillations and spindles. 9 Proc Natl Acad Sci USA 2018;115. https://doi.org/10.1073/pnas.1805517115.
[17] Peyrache A, Battaglia FP, Destexhe A. Inhibition recruitment in prefrontal cortex during sleep spindles and gating of hippocampal inputs. 10 Proc Natl Acad Sci USA 2011;108:17207–12.
[18] Niethard N, Burgalossi A, Born J. Plasticity during sleep is linked to specific regulation of cortical circuit activity. 9 Front Neural Circ 2017;11. https://doi.org/10.3389/fncir.2017.00065.
[19] Zrenner C, Desideri D, Belardinelli P, Ziemann U. Real-time EEG-defined excitability states determine efficacy of TMS-induced plasticity in human motor cortex. Brain Stimul 2018;11:374–89.
[20] Bergmann TO, Lieb A, Zrenner C, Ziemann U. Pulsed facilitation of corticospinal excitability by the sensorimotor μ-alpha rhythm. 12 J Neurosci: The Official Journal of the Society for Neuroscience 2019;39:10034–43.
[21] Bergmann TO, Molle M, Schmidt MA, Lindner C, Marshall L, Born J, Siebner HR. EEG-guided transcranial magnetic stimulation reveals rapid shifts in motor cortical excitability during the human sleep slow oscillation. 1 J Neurosci 2012;32:243–53.
[22] Hassan U, Feld GB, Bergmann TO. Automated real-time EEG sleep spindle detection for brain-state-dependent brain stimulation. 9 Journal of Sleep Research 2022. https://doi.org/10.1111/jsr.13733.
[23] Rossi S, Hallett M, Rossini PM, Pascual-Leone A. Screening questionnaire before TMS: an update. 8 Clin Neurophysiol: Official Journal of the International Federation of Clinical Neurophysiology 2011;122:1686.
[24] Hassan U, Pillen S, Zrenner C, Bergmann TO. The Brain Electrophysiological recording & STimulation (BEST) toolbox. 1 Brain Stimul 2022;15:109–15.
[25] Avesani M, Formaggio E, Fuggetta G, Fiaschi A, Manganotti P. Corticospinal excitability in human subjects during nonrapid eye movement sleep: single and paired-pulse transcranial magnetic stimulation study. 5 Experimental Brain Research. Experimentelle Hirnforschung. Experimentation Cerebrale 2008;187:17–23.
[26] Grosse P, Khatami R, Salih F, Kuhn A, Meyer B-U. Corticospinal excitability in human sleep as assessed by transcranial magnetic stimulation. 12 Neurology 2002;59:1988–91.
[27] Salih F, Khatami R, Steinheimer S, Hummel O, Kühn A, Grosse P. Inhibitory and excitatory intracortical circuits across the human sleep-wake cycle using paired-pulse transcranial magnetic stimulation. 6 J Physiol 2005;565:695–701.
[28] Russo S, Sarasso S, Puglisi GE, Palù DD, Pigorini A, Casarotto S, D'Ambrosio S, Astolfi A, Massimini M, Rosanova M, Fecchio M. Taac - TMS Adaptable Auditory Control: a universal tool to mask TMS clicks. 3 J Neurosci Methods 2022;370:109491.
[29] Hassanzahraee M, Zoghi M, Jaberzadeh S. Longer transcranial magnetic stimulation intertrial interval increases size, reduces variability, and improves the reliability of motor evoked potentials. 12 Brain Connect 2019;9:770–6.
[30] Vallat R, Walker MP. An open-source, high-performance tool for automated sleep staging. 10 Elife 2021;10. https://doi.org/10.7554/eLife.70092.
[31] Zrenner C, Galevska D, Nieminen JO, Baur D, Stefanou M-I, Ziemann U. The shaky ground truth of real-time phase estimation. 7 Neuroimage 2020;214:116761.
[32] Gramfort A, Luessi M, Larson E, Engemann DA, Strohmeier D, Brodbeck C, Parkkonen L, Hämäläinen MS. MNE software for processing MEG and EEG data. 2 Neuroimage 2014;86:446–60.
[33] Oostenveld R, Fries P, Maris E, Schoffelen J-M. FieldTrip: open source software for advanced analysis of MEG, EEG, and invasive electrophysiological data. Comput Intell Neurosci 2011;2011:156869.
[34] Carrier J, Viens I, Poirier G, Robillard R, Lafortune M, Vandewalle G, Martin N, Barakat M, Paquet J, Filipini D. Sleep slow wave changes during the middle years of life. 2 Eur J Neurosci 2011;33:758–66.
[35] Massimini M, Huber R, Ferrarelli F, Hill S, Tononi G. The sleep slow oscillation as a traveling wave. 8 J Neurosci 2004;24:6862–70.
[36] Donoghue T, Haller M, Peterson EJ, Varma P, Sebastian P, Gao R, Noto T, Lara AH, Wallis JD, Knight RT, Shestyuk A, Voytek B. Parameterizing neural power spectra into periodic and aperiodic components. 12 Nat Neurosci 2020;23:1655–65.
[37] Thies M, Zrenner C, Ziemann U, Bergmann TO. Sensorimotor mu-alpha power is positively related to corticospinal excitability. 9 Brain Stimul 2018;11:1119–22.
[38] Virtanen P, Gommers R, Oliphant TE, Haberland M, Reddy T, Cournapeau D, Van Mulbregt P. SciPy 1.0: fundamental algorithms for scientific computing in Python. Nat Methods 2020;17(3):261–72.
[39] Berens P. CircStat: a MATLAB toolbox for circular statistics. J Stat Software 2009;31:1–21.
[40] Schaworonkow N, Triesch J, Ziemann U, Zrenner C. EEG-triggered TMS reveals stronger brain state-dependent modulation of motor evoked potentials at weaker stimulation intensities. 1 Brain Stimul 2019;12:110–8.
[41] Stefanou M-I, Desideri D, Belardinelli P, Zrenner C, Ziemann U. Phase synchronicity of μ-rhythm determines efficacy of interhemispheric communication between human motor cortices. 12 J Neurosci: The Official Journal of the Society for Neuroscience 2018;38:10525–34.
[42] Wischnewski M, Haigh ZJ, Shirinpour S, Alekseichuk I, Opitz A. The phase of sensorimotor mu and beta oscillations has the opposite effect on corticospinal excitability. 9 Brain Stimul 2022;15:1093–100.
[43] Ozdemir RA, Kirkman S, Magnuson JR, Fried PJ, Pascual-Leone A, Shafi MM. Phase matters when there is power: phasic modulation of corticospinal excitability occurs at high amplitude sensorimotor mu-oscillations. 12 Neuroimage: Report 2022;2:100132.
[44] Zrenner C, Belardinelli P, Ermolova M, Gordon PC, Stenroos M, Zrenner B, Ziemann U. μ-rhythm phase from somatosensory but not motor cortex correlates with corticospinal excitability in EEG-triggered TMS. 9 J Neurosci Methods 2022;379:109662.
[45] Zrenner C, Kozák G, Schaworonkow N, Metsomaa J, Baur D, Vetter D, Blumberger DM, Ziemann U, Belardinelli P. Corticospinal excitability is highest at the early rising phase of sensorimotor μ-rhythm. Neuroimage 2023;266:119805.
[46] Antony JW, Piloto L, Wang M, Pacheco P, Norman KA, Paller KA. Sleep spindle refractoriness segregates periods of memory reactivation. Curr Biol: CB 2018;28:1736–1743.e4.
[47] Koupparis AM, Kokkinos V, Kostopoulos GK. Spindle power is not affected after spontaneous K-complexes during human NREM sleep. 1 PLoS One 2013;8:e54343.
[48] Gardner RJ, Hughes SW, Jones MW. Differential spike timing and phase dynamics of reticular thalamic and prefrontal cortical neuronal populations during sleep spindles. 11 J Neurosci 2013;33:18469–80.
[49] Fernandez LMJ, Vantomme G, Osorio-Forero A, Cardis R, Béard E, Lüthi A. Thalamic reticular control of local sleep in mouse sensory cortex. 12 Elife 2018;7. https://doi.org/10.7554/eLife.39111.
[50] Raven F, Aton SJ. The engram's dark horse: how interneurons regulate state-dependent memory processing and plasticity. 9 Front Neural Circ 2021;15. https://doi.org/10.3389/fncir.2021.750541.
[51] Thankachan S, Katsuki F, McKenna JT, Yang C, Shukla C, Deisseroth K, Uygun DS, Strecker RE, Brown RE, McNally JM, Basheer R. Thalamic reticular nucleus parvalbumin neurons regulate sleep spindles and electrophysiological aspects of schizophrenia in mice. 12 Sci Rep 2019;9:3607.
[52] Dickey CW, Sargsyan A, Madsen JR, Eskandar EN, Cash SS, Halgren E. Travelling spindles create necessary conditions for spike-timing-dependent plasticity in humans. 12 Nat Commun 2021;12:1027.
[53] Ayoub A, Mölle M, Preissl H, Born J. Grouping of MEG gamma oscillations by EEG sleep spindles. Neuroimage 2012;59(2):1491–500.
[54] Jiang X, Gonzalez-Martinez J, Halgren E. Posterior hippocampal spindle ripples Co-occur with neocortical theta bursts and downstates-upstates, and phase-lock with parietal spindles during NREM sleep in humans. J Neurosci: The Official Journal of the Society for Neuroscience 2019;39:8949–68.
[55] Staresina BP, Bergmann TO, Bonnefond M, van der Meij R, Jensen O, Deuker L, Elger CE, Axmacher N, Fell J. Hierarchical nesting of slow oscillations, spindles and ripples in the human hippocampus during sleep. 11 Nat Neurosci 2015;18:1679–86.
[56] Sirota A, Csicsvari J, Buhl D, Buzsáki G. 2. Communication between neocortex and hippocampus during sleep in rodents, vol. 100. Proceedings of the National Academy of Sciences; 2003. p. 2065–9.
[57] Feldman DE. The spike-timing dependence of plasticity. 8 Neuron 2012;75:556–71.
[58] Rosanova, M. (10 2005). Pattern-specific associative long-term potentiation induced by a sleep spindle-related spike train. J Neurosci, 25, 9398–9405.
[59] Helfrich RF, Mander BA, Jagust WJ, Knight RT, Walker MP. Old brains come uncoupled in sleep: slow wave-spindle synchrony, brain atrophy, and forgetting. 1 Neuron 2018;97:221–230.e4.
[60] Huerta PT, Lisman JE. Bidirectional synaptic plasticity induced by a single burst during cholinergic theta oscillation in CA1 in vitro. Neuron 1995;15:1053–63.
[61] Niethard N, Hasegawa M, Itokazu T, Oyanedel CN, Born J, Sato TR. Sleep-stage-specific regulation of cortical excitation and inhibition. 10 Curr Biol: CB 2016;26:2739–49.
[62] Niethard N, Brodt S, Born J. Cell-type-specific dynamics of calcium activity in cortical circuits over the course of slow-wave sleep and rapid eye movement sleep. 5 J Neurosci: The Official Journal of the Society for Neuroscience 2021;41:4212–22.
[63] Baur D, Galevska D, Hussain S, Cohen LG, Ziemann U, Zrenner C. Induction of LTD-like corticospinal plasticity by low-frequency rTMS depends on pre-stimulus phase of sensorimotor μ-rhythm. 11 Brain Stimul 2020;13:1580–7.
[64] Baur D, Ermolova M, Souza VH, Zrenner C, Ziemann U. Phase-amplitude coupling in high-gamma frequency range induces LTP-like plasticity in human motor cortex: EEG-TMS evidence. 11 Brain Stimul 2022. https://doi.org/10.1016/j.brs.2022.11.003.
[65] Ross JM, Forman L, Gogulski J, Hassan U, Cline CC, Parmigiani S, Truong J, Hartford JW, Chen NF, Fujioka T, Makeig S. Sensory Entrained TMS (seTMS) enhances motor cortex excitability. bioRxiv 2024;2024:11.
[66] Cash RFH, Murakami T, Chen R, Thickbroom GW, Ziemann U. Augmenting plasticity induction in human motor cortex by disinhibition stimulation. 1 Cerebr Cortex 2016;26:58–69.
[67] Rasch B, Born J. About sleep's role in memory. 4 Physiol Rev 2013;93:681–766.
[68] Mölle M, Marshall L, Gais S, Born J. Grouping of spindle activity during slow oscillations in human non-rapid eye movement sleep. J Neurosci: The Official Journal of the Society for Neuroscience 2002;22(24):10941–7.
[69] Mölle M, Bergmann TO, Marshall L, Born J. Fast and slow spindles during the sleep slow oscillation: disparate coalescence and engagement in memory processing. 10 Sleep 2011;34:1411–21. https://doi.org/10.5665/SLEEP.1290.
[70] Hahn MA, Heib D, Schabus M, Hoedlmoser K, Helfrich RF. Slow oscillation-spindle coupling predicts enhanced memory formation from childhood to adolescence. 6 Elife 2020;9. https://doi.org/10.7554/eLife.53730.

[71] Latchoumane C-FV, Ngo H-VV, Born J, Shin H-S. Thalamic spindles promote memory formation during sleep through triple phase-locking of cortical, thalamic, and hippocampal rhythms. Neuron 2017;95(2):424–35. e6.
[72] Gordon PC, Jovellar DB, Song Y, Zrenner C, Belardinelli P, Siebner HR, Ziemann U. Recording brain responses to TMS of primary motor cortex by EEG–utility of an optimized sham procedure. Neuroimage 2021;245:118708.
[73] Desideri D, Zrenner C, Ziemann U, Belardinelli P. Phase of sensorimotor μ-oscillation modulates cortical responses to transcranial magnetic stimulation of the human motor cortex. The Journal of physiology 2019;597(23):5671–86.